ChemistryOpen

Research Article
doi.org/10.1002/open.202200118

Chemistry Europe
European Chemical Societies Publishing

www.chemistryopen.org

Be_3Ru: Polar Multiatomic Bonding in the Closest Packing of Atoms

Laura Agnarelli, Yurii Prots, Marcus Schmidt, Mitja Krnel, Eteri Svanidze, Ulrich Burkhardt, Andreas Leithe-Jasper,* and Yuri Grin[a]

The new phase Be_3Ru crystallizes with $TiCu_3$-type structure (space group *Pmmn* (59), $a = 3.7062(1)$ Å, $b = 4.5353(1)$ Å, $c = 4.4170(1)$ Å), a coloring variant of the hexagonal closest packing (*hcp*) of spheres. The electronic structure revealed that Be_3Ru has a pseudo-gap close to the Fermi level. A strong charge transfer from Be to Ru was observed from the analysis of electron density within the Quantum Theory of Atoms in Molecules (QTAIM) framework and polar three- and four-atomic Be−Ru bonds were observed from the ELI–D (electron localizability indicator) analysis. This situation is very similar to the recently investigated Be_5Pt and $Be_{21}Pt_5$ compounds. The unusual crystal chemical feature of Be_3Ru is that different charged species belong to the same closest packing, contrary to typical inorganic compounds, where the cationic components are located in the voids of the closest packing formed by anions. Be_3Ru is a diamagnet displaying metallic electrical resistivity.

Introduction

Beryllium finds different technological applications as elemental metal (e.g., X-ray windows, satellite mirrors or nuclear shields) or as alloying component in diverse light-weight materials. Despite this, the knowledge of beryllium-containing intermetallic compounds is scanty in comparison with other series of intermetallic compounds. Moreover, the crystal chemistry of beryllium intermetallic compounds is barely investigated, its binary and ternary phase diagrams are scarcely studied and only the industrially relevant ones have been explored. This is mainly due to the challenges associated with preparation, characterization and the notorious toxicity of beryllium.[1] In general, the structural chemistry of beryllium intermetallic compounds is governed by the relatively small atomic radius, low valence electron count, and covalent character of beryllium. Moreover, the relatively small size of beryllium atoms leads to higher coordination numbers, especially for the beryllium-rich phases.[2]

Beryllium is a good electrical conductor with the bulk superconductivity observed below $T_c = 0.026$ K. Superconductivity was also reported for several beryllium intermetallic compounds, an example is the recently discovered $Be_{21}Pt_5$ – one of the few complex metallic alloys displaying superconductivity below $T_c = 2.06$ K.[3] In contrast to typical intermetallic compounds, a study on Be_5Pt revealed a semiconducting behavior at very low valence-electron count.[4] From a chemical point of view, in order to obtain an intermetallic compound with semiconducting characteristics, that is, showing a narrow gap at the Fermi level, some criteria regarding the combination of different bonding types between the components should be fulfilled (Figure 1). Noteworthy examples of semiconductors are the elements belonging to the *p* block (e.g. Ge and Si). A combination of elements from the group 13 with those from the group 15 or between elements from group 12 with those from group 16, can give rise to semiconducting materials – for example GaAs[5] or ZnSe,[6] which are characterized by two-center-two-electron moderately polar bonds. Moving to the left side of the Periodic Table, where the number of electrons in the last shell (ELSA[7]) is reduced, different bonding scenarios can be observed, depending on the difference in electronegativity between the components. When the difference in electro-

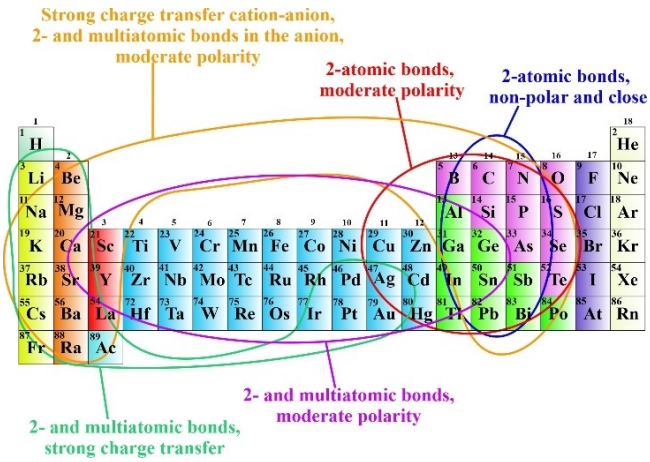

Figure 1. Different kinds of chemical bonding in semiconducting elements and compounds.

[a] *L. Agnarelli, Dr. Y. Prots, Dr. M. Schmidt, Dr. M. Krnel, Dr. E. Svanidze, Dr. U. Burkhardt, Dr. A. Leithe-Jasper, Prof. Dr. Y. Grin*
Chemische Metallkunde
Max-Planck-Institut für Chemische Physik fester Stoffe
Nöthnitzer Straße 40
01187 Dresden (Germany)
E-mail: Andreas.Leithe-Jasper@cpfs.mpg.de

Supporting information for this article is available on the WWW under https://doi.org/10.1002/open.202200118

negativity is very large, Zintl phases are the protagonists: the cationic part donates its valence electrons to the anionic one to form two center- and/or multiatomic bonds with moderate polarity in the anion sublattices. The anionic part of the Zintl phases is preferably formed by elements belonging to the *p* block, combined with elements of low electronegativity belonging to the 1–3 groups (e.g., $SrSi_2$,[8] $BaSi_2$[9]). Such materials show mostly gaps or pseudo-gaps in the electronic density of states (DOS) near the Fermi level. Compounds of late transition metals and alkaline or earth alkaline metals (e.g., Cs_2Pt,[10] RbAu[11]) or with elements belonging to the *p* block (e.g., $FeGa_3$,[12] $RuGa_3$[13]) can also show a gap at the Fermi level. While in the first family -aurides and platinates – the gap may be large here, it is essentially smaller in the second family. In the former, the difference in electronegativity between the components is high, suggesting the formation of ionic, polar two- and multi-atomic bonds; in the second, the difference in electronegativity is not so high, encouraging the formation of two- and multi-atomic bonds with moderate polarity. The last two groups represent relatively rare cases among materials with semiconducting properties. During the recent studies on the Be–Pt system, it was found that Be_5Pt is a semiconductor,[4] belonging to the first of the last two groups mentioned above. Motivated by this interesting result, we decided to investigate the Be–Ru system, with the aim of finding new semiconducting materials. Differently from what we expected, the new phase reported here, Be_3Ru, does not show semiconducting behavior, being a metal. It shows an unusual crystal chemical feature, representing a closest packing structure formed by differently charged species.

Results and Discussion

The existence of a phase with composition $Be_{10}Ru_3$ was first suggested by Obrowski[14] who claimed that it is of γ-brass type, crystallizing with the cubic Cu_5Zn_8-type structure. Analysis of X-ray diffraction data measured on the single crystals selected from the sample with the nominal composition Be_3Ru (cf. Experimental Section), revealed instead an orthorhombic lattice, and the systematic extinctions were compatible with the space group *Pmmn* (Table 1).

The crystal structure contains three crystallographically unique atoms in the unit cell (Table 2), which includes two different Be and one Ru site. The structure was refined with anisotropic displacement parameters only for the heavy Ru atom. The refinement shows that all sites are fully occupied. Be_3Ru crystallizes with $TiCu_3$-type structure.[15] The final difference Fourier map did not reveal significant residual density. The refined atomic coordinates, together with the atomic displacement parameters, are listed in Table 2. Information about the interatomic distances and coordination numbers of the atoms can be found in Table 1S (Supporting Information). The crystallographic data are deposited in the ICSD database with deposition number 2169466.

The crystal structure of Be_3Ru can be derived from a distorted hexagonal structure ($2c/b = 1.947$ instead of $\sqrt{3} = 1.732$) in which the atoms are organized in closest-packed layers perpendicular to [100], in an *hcp* sequence *ABAB*…[16] Typically for closest-packed structures, the coordination number for all the atoms is 12, and the coordination polyhedra around Be and Ru atoms are distorted hexagonal analogues of cuboctahedra (anticuboctahedra, Figures 2 and 1S). Ru atoms are found at a rather long distance of 3.12 Å from each other (longer than 2.65 Å, the Ru–Ru distance in elemental Ru),[17] therefore there are no homoatomic Ru–Ru contacts in the structure. The coordination environment of Ru is made only of Be atoms. The anticuboctahedron around Be1 atom contains 4 Ru, 4 Be1, and 4 Be2 atoms, while the one around Be2 atom contains 4 Ru and 8 Be1 atoms. The anticuboctahedra are condensed by sharing the triangular faces and form infinite columns along [100]. The columns are shifted with respect to each other along [100] in a way that the anticuboctahedra belonging to one column share the rectangular faces with the anticuboctahedra belonging to the second column (Figure 2).[18] The Be–Ru bond lengths range from 2.29 Å to 2.57 Å, which can

Table 1. Crystallographic data for Be_3Ru.

Composition	Be_3Ru
Space group	*Pmmn*
Pearson symbol	*oP*8
Formula units per u.c. *Z*	2
Unit cell parameters[a]	
a(Å)	3.7062(1)
b(Å)	4.5353(1)
c(Å)	4.4170(1)
V(Å^3)	74.244(6)
Calculated density ρ (g cm^{-3})	5.72
Crystal form	Irregular shape
Crystal size (mm^3)	0.030×0.035×0.050
Diffraction system	RIGAKU AFC7
Detector	Saturn 724+ CCD
Radiation, wavelength	Mo*K*α, 0.71073 Å
Scan type; step per degree	ϕ; 0.6
N(images) measured	600
$2\theta_{max}$	60.06
Range in *hkl*	$-5 \le h \le 4$ $-6 \le k \le 6$ $-6 \le l \le 2$
Absorption correction	multi-scan
Absorption coefficient (mm^{-1})	9.8
T(max)/*T*(min)	1.75
N(*hkl*) measured	288
N(*hkl*) unique	125
R(int)	0.0136
N(*hkl*) observed	125
Observation criterion	$F(hkl) \ge 4\sigma$ [F(*hkl*)]
R_F, R_w	0.0251, 0.0270
Largest diff. peak and hole (e$^-$ Å^{-3})	−0.5/0.6

[a] X-ray powder diffraction data.

Table 2. Atomic coordinates and displacement parameters for Be_3Ru (space group *Pmmn*).

Atom	Site	*x/a*	*y/b*	*z/c*	$U_{eq}/_{iso}$ [Å^2] [a]
Be1	4*e*	1/4	0.997(3)	0.646(2)	0.010(2)
Be2	2*a*	1/4	1/4	0.192(4)	0.015(3)
Ru	2*b*	3/4	1/4	0.8772(2)	0.0066(3)[b]

[a] $U_{eq} = 4/3\ [U_{11}\ (a^*)^2\ a^2 + \cdots 2U_{23}\ (b^*)\ (c^*)\ b\ c\ cos(\alpha)]$. [b] For Ru $U_{11} = 0.0085(5)$, $U_{22} = 0.0066(5)$, $U_{33} = 0.0048(4)$, $U_{ij} = 0$.

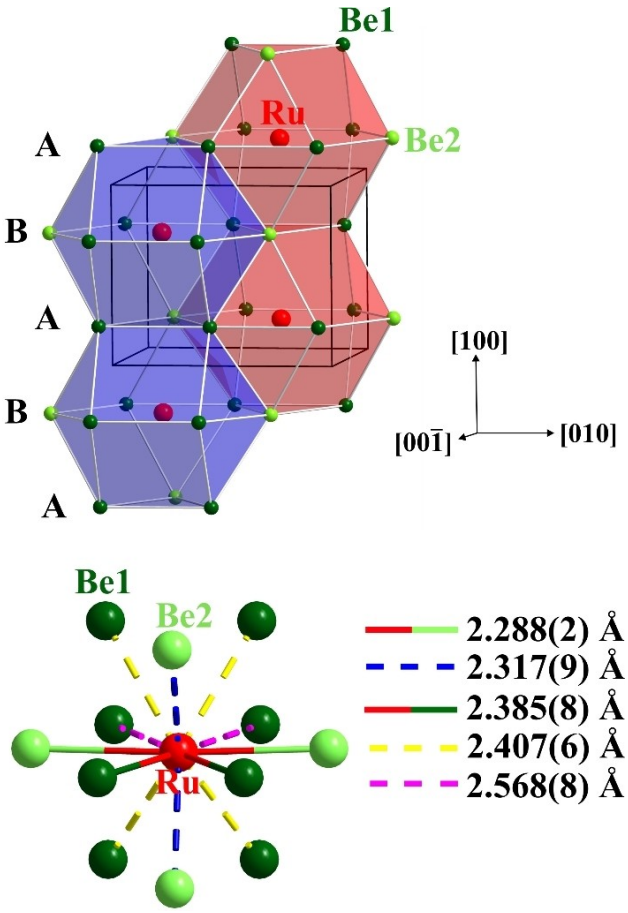

Figure 2. (top) Closest-packed layers perpendicular to [100] in the crystal structure of Be_3Ru. Two shifted columns of polyhedra around Ru stacked along [100] are shown in blue and red. (bottom) Interatomic distances around the Ru atom: dashed lines – the longest Ru–Be1 and Ru–Be2 distances; red-light green lines – the shortest Ru–Be2 distances; red-dark green lines – the shortest Ru–Be1 distances.

be interpreted using the covalent or atomic (metallic) radii, or combining both of them. Moreover, the Be1–Be2 distance of 2.28 Å is longer than the Be1–Be1 distance (2.24 Å) and is also longer than the distance of 2.08 Å in elemental Be.[17] The coordination environment of Be2 atoms contains only one type of Be atom (8 Be1) and 4 Ru atoms, while the coordination environment of Be1 atoms contains 4 Be1, 4 Be2, and 4 Ru atoms (Figure 1S).

The crystal structure of Be_3Ru belongs to the $TiCu_3$-type structure.[15,19] With the 118 representatives,[20] it is one of the basic structural prototypes of intermetallic compounds. The members of the $TiCu_3$ family are mainly formed by elements with similar electronegativities, like MNi_3 (M = Mo, Nb, Ta)[21] or the electronegativity of the majority component is higher, like in $REAu_3$ (RE = Gd–Lu).[22] The atomic arrangement in $TiCu_3$ (Be_3Ru, space group *Pmmn*), together with that of Mg_3Cd ($P6_3/mmc$), represents a superstructure ('coloring' variant) of the hexagonal closest packing (*hcp*) of spheres. Both basic structure types differ in the ordering pattern within the closest packed layer - orthorhombic in $TiCu_3$, and hexagonal in Mg_3Cd. Such way of 'coloring' opens a possibility to form a variety of potential intermediate structures with the component ratio 1:3.[16b] All these circumstances would likely yield a characteristic metallic band structure with non-vanishing electronic density of states (DOS) at the Fermi level.

The band structure calculations in semi- and full-relativistic approximation indeed reveal a non-zero DOS at the Fermi level E_F (Figure 3). Similar to other compounds of the transition metals with the *s* and *p* elements, the total electronic DOS is composed of three regions. The low-energy region ($E < -6$ eV) is formed mainly by the *s* states of Be with some admixtures of the Be–*p* and Ru–*d* and -*s* states. The *d* states of Ru make the majority contribution to the intermediate range (-6 eV $< E <$ -1.3 eV). While the separation of the first and second regions is not very pronounced, the third part can be clearly recognized just below the Fermi level (-1.3 eV $< E < E_F$), being mainly formed by a mixture of the Ru–*d* and Be2-*p* states. The strong structuring of the electronic DOS, in particular in the two last regions, indicates special features of the chemical bonding. Furthermore, in contrast to typical metallic materials, the electronic DOS of Be_3Ru shows a clear dip in the vicinity of the Fermi level. This resembles Zintl- and Wade-type phases (cf. $SrGe_6$,[23] $Sr_3Li_5Ga_5$,[24] $Ca_2Ga_4Ge_6$,[25] $Dy(Cu_{0.18}Ga_{0.82})_{3.7}$[26]) more than 'classical' intermetallic compounds.[27] On the other hand, the DOS of Be_3Ru in the vicinity of the Fermi level is similar to that of the recently investigated $Be_{21}Pt_5$[3] and Be_5Pt compounds,[4] which show a strong electron transfer from Be to Pt. The non-zero value of the DOS at the Fermi level E_F is consistent with metallic-type behavior of the electrical resistivity (Figure 4S, Supporting Information).

These DOS features, in combination with a low electron number in the last shell per atom (ELSA[7,28]) raise questions about their origin from the point of view of chemical bonding interaction.

The analysis of chemical bonding was performed by quantum chemical techniques in position space, which has recently been shown to be a powerful bonding investigation tool, in particular for intermetallic compounds with low ELSA and multi-atomic bonding.[3–4,7] The effective charges of all atoms were determined from the calculated electron density.

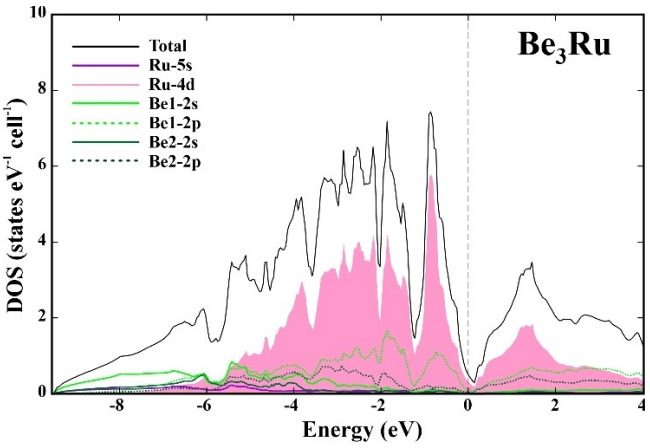

Figure 3. Calculated electronic density of states (DOS) of Be_3Ru, together with the partial contributions of relevant atomic states.

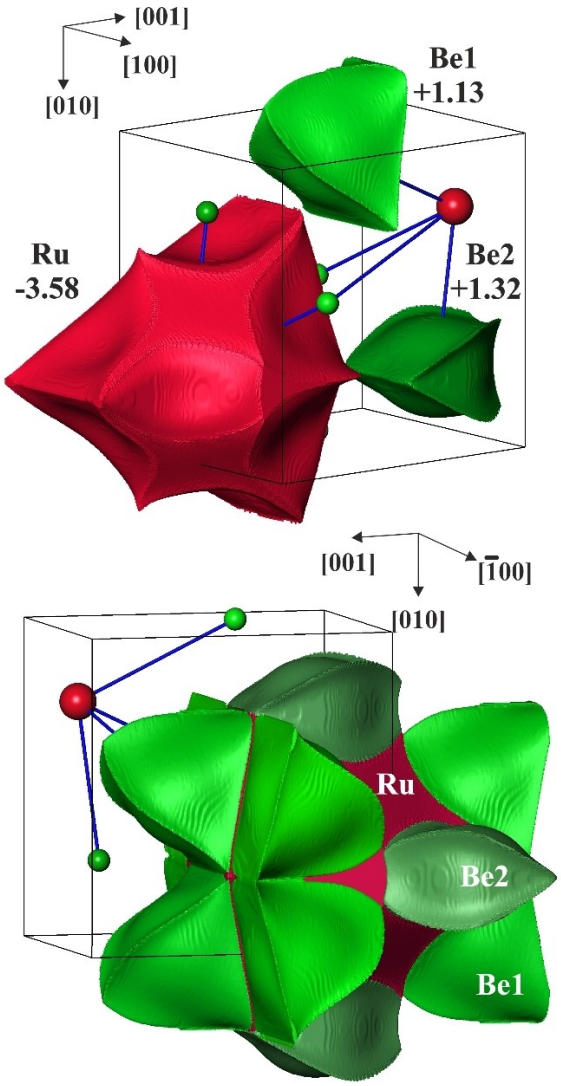

Figure 4. (top) QTAIM atomic shapes and charges in Be_3Ru. (bottom) Arrangement of the atomic beryllium basins around the ruthenium one. Free space on the red surface is used for direct contacts between the Ru atoms. Black lines show the unit cell, blue lines visualize the shortest Be–Ru contacts.

First, the zero-flux surfaces in the gradient vector field of the electron density were determined. They form the boundaries of electron density basins, which represent atomic regions according to the Quantum Theory of Atoms in Molecules (QTAIM).[29] The shape of the QTAIM Ru species in Be_3Ru reveals some characteristic features (Figure 4, top). It is far from a spherical one and has concave surfaces toward neighboring beryllium species, similar to the platinum and beryllium atoms in $Be_{21}Pt_5$[3] or iridium and magnesium atoms in $Mg_3Ga_{1-x}Ir_{3+x}$,[7] where this feature is correlated with the strong charge transfer. The beryllium species look like 'soft tetrahedrons' resembling atomic shapes of Be and Mg in the two above-mentioned compounds. Taking into account the twelve-coordination of Ru by Be, one may expect that the Ru QTAIM shapes do not contact each other. Nevertheless, plane common surfaces between neighboring Ru atoms are observed in Be_3Ru (Figure 4, bottom), indicative also of the Ru–Ru interactions in some form (cf. orange bonding basin in Figure 5).

In the next step, the electron density was integrated in spatial regions, defined above as atomic shapes, yielding their electronic population. Subtraction of the electron numbers in the neutral atoms (atomic number) from the latter results in the QTAIM effective atomic charges. Ruthenium atoms reveal a large negative charge of −3.58. The beryllium species are clearly playing the role of cations in Be_3Ru. In particular, Be2 – found at the shorter distance to Ru (2.29 Å) – shows a larger charge of +1.32, while Be1, found at a greater distance from Ru

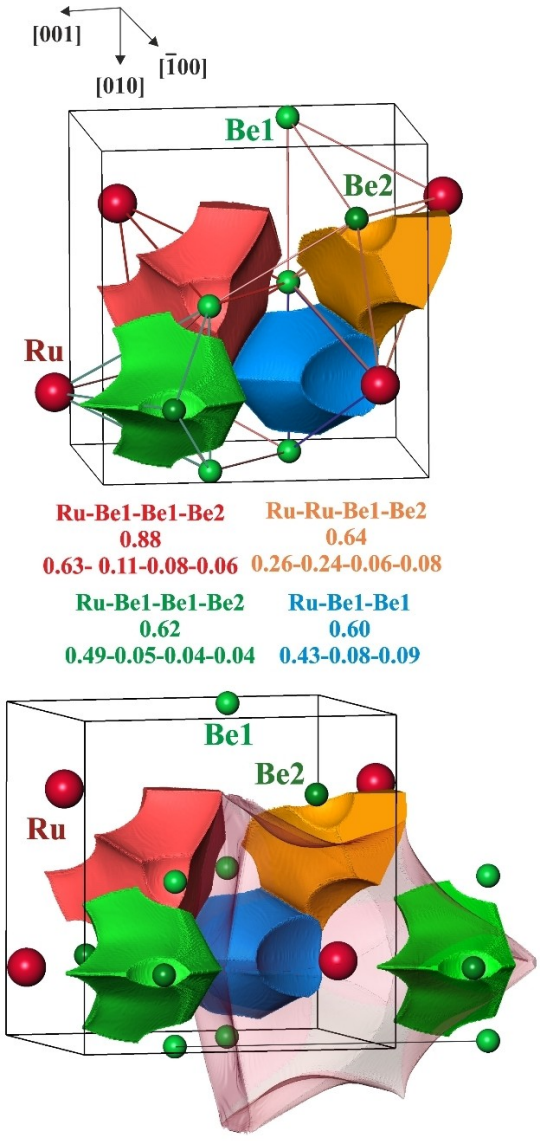

Figure 5. Electron localizability indicator in Be_3Ru: (top) shapes of four- (green, red and orange) and three-synaptic (blue) ELI–D bonding basins showing the multiatomic character of chemical bonding; (middle) atoms participating at the bonding basins (first line), populations of the bonding basins (in e^-, second line) and contributions of the participating atoms (third line), revealing polar character of the interactions; (bottom) intersection of the QTAIM atomic basin of Ru (transparent) with the ELI–D bonding basins (green, blue and orange), showing the majority of the volume of the bonding basins within the QTAIM atomic basin of ruthenium.

(2.38 Å), shows a smaller charge of +1.13. This variation indicates the different roles of Be1 and Be2 in the structural organization of Be_3Ru. In addition, the diamagnetic properties (Figure 5S, Supporting Information) of Be_3Ru might be also be related to such a charge transfer.

Further information about the bonding between atoms was obtained by applying the electron localizability approach,[30] based on the combined analysis of electron-localizability indicator and electron density. The electron localizability indicator (ELI–D) shows spherical distribution around the nuclei of the non-interacting (isolated) atoms. Due to the bonding interaction, the spherical distribution is violated and attractors may appear in the regions of valence or penultimate shells, signaling bonding and indicating its geometrical organization.[30] Each of the so-formed attractors has its own ELI–D basin, which is determined, like the QTAIM atomic basins, by the zero-flux surfaces in the gradient vector field of ELI–D. The number of common surfaces of a bonding basin with the attached core (penultimate shell) basins defines the synapticity of the bonding basin and characterizes the number of atomic species participating in this bond (bond atomicity). In Be_3Ru, only four types of bonding basins are observed, visualizing different components of bonding. The basins of the first group involve one Ru and three Be atoms and characterize the respective four-atomic bonds (red and green in Figure 5, top). The basins of the second group characterize the three-atomic bonding of one Ru and two Be species (blue, Figure 5). The basins of the third type (Figure 5, orange) involve two Ru and two beryllium atoms and highlight the Ru–Ru interaction, which is already indicated by an analysis of the electron density (see above), but within a four-atomic bond. The population of all bonding basins is formed mainly by the Ru atoms with minor contributions from the beryllium species (Figure 5, middle), indicating the pronounced polar character of bonding in Be_3Ru. This can be confirmed on the level of atomic volumes (Figure 5, bottom panel), where most parts of the volumes of bonding basins is located within the QTAIM atomic volume of ruthenium. For the quantitative characterization of the bond polarity for multi-atomic interactions, the concept of bonding polarity in position space[31] may be expanded from the two-atomic to multi-atomic bonds if only two sorts of atoms are participating in this bonding. Less dependent on the number of participating atoms, the polarity[32] of the Be–Ru interactions in Be_3Ru varies from 0.44 (red and blue basins in Figure 5) to 0.56 (orange basin) and 0.58 (green basin) on a scale between 0 (non-polar, covalent bond) and 1 (close-shell configuration, ionic bond). This is consistent with the pronounced charge transfer (cf. QTAIM charges discussed above, Figure 4).

Conclusion

Be_3Ru is one of the rare representatives of the $TiCu_3$-type structure, formed by the valence electron-poor element as a majority component. From the geometric point of view, the crystal structure of Be_3Ru can be derived by 'coloring' the hexagonal closest packing of spheres characteristic for large groups of intermetallic compounds. This is consistent with the low number of electrons in the last shell per atom (ELSA), typical for 'metallic' structures. Be_3Ru is a diamagnet and its metallic electrical resistivity is confirmed by electronic structure calculations as well as experimental measurements. The pseudo-gap in the DOS is however, unusual. The calculated QTAIM charges of −3.58 for Ru and +1.13 or +1.32 for Be reveal strong charge transfer. Both observations can be explained by the formation of polar three- and four-atomic Be–Ru bonds. The closest packing in Be_3Ru is jointly formed by cationic and anionic components. This is in contrast to traditional inorganic compounds where one of the components forms the closest-packing motif, while the other one is located in the voids of the previous one.

Experimental Section

Complete sample preparation was performed in a laboratory specialized for work with Be, inside an argon-atmosphere glove-box system (MBraun, $p(H_2O/O_2) < 0.1$ ppm).[33] Polycrystalline samples with nominal composition Be_3Ru were synthetized by arc melting from elemental Be (sheets, Heraeus, 99.2 wt%) and pre-melted Ru powder (Alfa Aesar, 99.95 wt%). To ensure the homogeneity, all samples were re-melted three times, with final mass losses of at most 5 wt%. To compensate for the beryllium loss during arc melting, a small excess (≈5 wt%) of the latter was used. The samples were placed into BeO crucibles and sealed in Ta tubes. In order to obtain single-phase material, several experiments with varied annealing time have been carried out. After annealing at 1300 °C for 1 day, impurities of the Be-rich neighbor phase were observed. Only after annealing for 7 days at 1300 °C, a single-phase material was obtained (Figure 2S and Figure 3S). Be_3Ru does not show an evident homogeneity range and does not exhibit air or moisture sensitivity. The thermal behavior of the prepared materials was studied in a differential scanning calorimeter (DSC) Netzsch DSC 404 C Pegasus, using a ZrO_2 crucible with lid, sealed in a Ta ampoule (purity of Ta 99.995%). The phase was found to decompose at 1510 °C.

Powder X-ray diffraction measurements were performed on a Huber G670 Image plate Guinier camera using LaB_6 as internal standard (Cu $K\alpha 1$ radiation, $\lambda = 1.54056$ Å; see Supporting Information). The lattice parameters were determined by a least-squares refinement using the peak positions, extracted by profile fitting.

Single crystals of Be_3Ru were selected from the crushed annealed samples. They were glued to thin glass fibers and were analyzed at room temperature using a Rigaku AFC7 diffraction system equipped with a Saturn 724+ CCD detector (Mo$K\alpha$ radiation, $\lambda =$ 0.71073 Å). Absorption correction was performed by a multi-scan procedure. All crystallographic calculations were made with the program package WinCSD.[34] Details and results of the data collection are listed in Table 1. The electrical and magnetic properties of Be_3Ru were determined experimentally from measurements on a few mm-sized irregular shaped solid chunk. Electrical resistivity measurements were performed by a Quantum Design Physical Property Measurement System (PPMS) 9 T, using a standard 4-terminal technique. Two Pt wires were used for making voltage contacts and two for current contacts. The wires were glued to the surface of the sample by using DuPont 4922 N silver conducting paste. Ac electrical resistivity ρ was measured at fixed temperatures between 2 and 300 K in 0 T and

9 T magnetic fields by applying 1 mA current pulse with frequency 23 Hz for 1 s. The measured data is shown in Figure 4S in Supporting Information. Magnetic measurements were conducted in a Quantum Design Magnetic Property Measurement System (MPMS) XL-5 superconducting quantum interference (SQUID) magnetometer equipped with a 7 T magnet. The sample was mounted on a capillary glass tube with varnish glue and its magnetic moment was measured vs. temperature in a stable magnetic field. The direct current (*dc*) magnetic susceptibility $\chi = M/H$ in the temperature range between 300 and 2 K for magnetic field $\mu_0 H = 1$ T, is shown in Figure 5S of Supporting Information.

Electronic structure calculations on Be_3Ru were performed by using the all-electron, full-potential local orbital (FPLO) method.[35] The experimental values of lattice parameters and the optimized values of atomic coordinates were used for calculations with a full relativistic model for the DOS and a semi-relativistic model for the electron density and ELI–D calculation. All results were obtained within the local density approximation (LDA) to the density functional theory through the Perdew-Wang parametrization for the exchange-correlation effects.[36] A mesh of $12\times12\times12$ *k* points was used for calculations.

The analysis of the chemical bonding was performed using the electron localizability approach in position space.[30c,37] For this purpose, the electron localizability indicator (ELI) in its ELI–D representation[30a,b] and the electron density (ED) were calculated with a specialized module within the FPLO code.[38] The topologies of the calculated three-dimensional distributions of ELI–D and ED were evaluated by means of the DGrid program.[39] The atomic charges from ED and bond populations for bonding basins from ELI–D were obtained via the integration of ED within the basins (space regions), bounded by zero-flux surfaces in the according gradient field. This procedure follows the Quantum Theory of Atoms in Molecules (QTAIM).[29]

Deposition Number 2169466 (for Be_3Ru) contains the supplementary crystallographic data for this paper. These data are provided free of charge by the joint Cambridge Crystallographic Data Centre and Fachinformationszentrum Karlsruhe Access Structures service.

Acknowledgements

We thank Dr. W. Carrillo-Cabrera, Dr. R. Cardoso and Dr. F. R. Wagner for helpful discussions. We express our gratitude to S. Scharsach for DTA measurements and K. Vanatko for the help in the laboratory work. We thank I. Werner for the help with information search.

Conflict of Interest

The authors declare no conflict of interest.

Data Availability Statement

The data that support the findings of this study are available from the corresponding author upon reasonable request.

Keywords: beryllium · hexagonal closest packing · intermetallic compound · polar multiatomic bonds · ruthenium

[1] a) D. Naglav, M. R. Buchner, G. Bendt, F. Kraus, S. Schulz, *Angew. Chem. Int. Ed.* **2016**, *55*, 10562–10576; *Angew. Chem.* **2016**, *128*, 10718–10733; b) O. Janka, R. Pöttgen, *Z. Naturforsch. B* **2020**, *75*, 421–439.
[2] A. Amon, in *Handbook on the Physics and Chemistry of Rare Earths, Vol. 59*, Elsevier, **2021**, pp. 93–140.
[3] A. Amon, A. Ormeci, M. Bobnar, L. G. Akselrud, M. Avdeev, R. Gumeniuk, U. Burkhardt, Y. Prots, C. Hennig, A. Leithe-Jasper, Y. Grin, *Acc. Chem. Res.* **2018**, *51*, 214–222.
[4] A. Amon, E. Svanidze, A. Ormeci, M. König, D. Kasinathan, D. Takegami, Y. Prots, Y.-F. Liao, K.-D. Tsuei, L. H. Tjeng, A. Leithe-Jasper, Y. Grin, *Angew. Chem. Int. Ed.* **2019**, *58*, 15928–15933; *Angew. Chem.* **2019**, *131*, 16075–16080.
[5] T. M. Quist, R. H. Rediker, R. Keyes, W. Krag, B. Lax, A. L. McWhorter, H. Zeigler, *Appl. Phys. Lett.* **1962**, *1*, 91–92.
[6] H. Morkoç, S. Strite, G. B. Gao, M. E. Lin, B. Sverdlov, M. Burns, *J. Appl. Phys.* **1994**, *76*, 1363–1398.
[7] O. Sichevych, Y. Prots, W. Schnelle, F. R. Wagner, Y. Grin, *Molecules* **2022**, *27*, 659.
[8] D. Shiojiri, T. Iida, M. Yamaguchi, N. Hirayama, Y. Imai, *Comput. Condens. Matter* **2022**, *30*, e00620.
[9] S. Kishino, T. Imai, T. Iida, Y. Nakaishi, M. Shinada, Y. Takanashi, N. Hamada, *J. Alloys Compd.* **2007**, *428*, 22–27.
[10] A. Karpov, J. Nuss, U. Wedig, M. Jansen, *Angew. Chem. Int. Ed.* **2003**, *42*, 4818–4821; *Angew. Chem.* **2003**, *115*, 4966–4969.
[11] M. Aycibin, E. Kilit Dogan, S. E. Gulebaglan, M. N. Secuk, B. Erdinc, H. Akkus, *Comput. Condens. Matter* **2014**, *1*, 32–37.
[12] F. R. Wagner, R. Cardoso-Gil, B. Boucher, M. Wagner-Reetz, J. Sichelschmidt, P. Gille, M. Baenitz, Y. Grin, *Inorg. Chem.* **2018**, *57*, 12908–12919.
[13] Y. V. Knyazev, Y. I. Kuz'min, *Phys. Solid State* **2017**, *59*, 2244–2247.
[14] W. Obrowski, *Metall* **1963**, *17*, 108–112.
[15] a) N. Karlsson, *Int. J. Mater. Res.* **1951**, *79*, 391–405; b) E. Raub, P. Walter, M. Engel, *Int. J. Mater. Res.* **1952**, *43*, 112–118.
[16] a) C. W. Fairhurst, J. B. Cohen, *Acta Crystallogr. Sect. B* **1972**, *28*, 371–378; b) Y. Grin, I. Zalutski, *Strojenie, swojstwa i primenenije metallidow* **1974**, 66–69; c) V. Paidar, D. Pope, M. Yamaguchi, *Scr. Metall.* **1981**, *15*, 1029–1031.
[17] J. Donohue, *Structures of the Elements*, John Wiley & Sons Inc, New York **1974**.
[18] a) W. Burkhardt, K. Schubert, *Int. J. Mater. Res.* **1959**, *50*, 442–452; b) W. A. Crichton, P. Bouvier, B. Winkler, A. Grzechnik, *Dalton Trans.* **2010**, *39*, 4302–4311; c) J. Sinclair, S. Baranets, S. Bobev, *Z. Kristallogr. Cryst. Mater.* **2021**, *236*, 61–70.
[19] K. H. J. Buschow, *Acta Metall.* **1983**, *31*, 155–160.
[20] P. Villars, K. Cenzual, *Pearson's Crystal Data* **2009**.
[21] a) T. Fang, S. J. Kennedy, L. Quan, T. J. Hicks, *J. Phys. Condens. Matter* **1992**, *4*, 2405–2414; b) E. Pylaeva, E. Gladyshevskii, P. Kripyakevich, *Zhur. Neorg. Khim* **1958**, *3*, 1626–1631.
[22] a) O. McMasters, K. Gschneidner Jr, G. Bruzzone, A. Palenzona, *J. Less-Common Met.* **1971**, *25*, 135–160; b) S. Saito, P. A. Beck, *Trans. Metall. Soc. AIME* **1959**, *215*, 938–941.
[23] U. Schwarz, R. Castillo, J. M. Hübner, A. Wosylus, Y. Prots, M. Bobnar, Y. Grin, *Z. Naturforsch. B* **2020**, *75*, 209–216.
[24] M. Kotsch, Y. Prots, A. Ormeci, A. Senyshyn, M. Kohout, Yu. Grin, *Z. Anorg. Allg. Chem.* **2021**, *647*, 1797–1803.
[25] K. L. Hodge, H. O. Davis, K. G. Koster, W. Windl, C. E. Moore, J. E. Goldberger, *Z. Anorg. Allg. Chem.*, e202100342.
[26] H. E. Mitchell Warden, S. B. Lee, D. C. Fredrickson, *Inorg. Chem.* **2020**, *59*, 10208–10222.
[27] a) R. Hoffmann, *Solids and Surfaces: A Chemist's View of Bonding in Extended Structures*, John Wiley & Sons, New York **2021**; b) P. Ravindran, R. Asokamani, *Bull. Mater. Sci.* **1997**, *20*, 613–622.
[28] Y. Grin, *Crystal Structure and Bonding in Intermetallic Compounds*, Elsevier, Amsterdam **2013**.
[29] R. F. W. Bader, *Atoms in Molecules: A Quantum Theory* Oxford University Press, Oxford, **1999**.
[30] a) M. Kohout, *Faraday Discuss.* **2007**, *135*, 43–54; b) M. Kohout, F. Wagner, Y. Grin, *Int. J. Quantum Chem.* **2006**, *106*, 1499–1507; c) F. R. Wagner, V. Bezugly, M. Kohout, Yu. Grin, *Chem. Eur. J.* **2007**, *13*, 5724–5741.

[31] a) D. Bende, F. R. Wagner, Y. Grin, *Inorg. Chem.* **2015**, *54*, 3970–3978; b) F. Wagner, D. Bende, Y. Grin, *Dalton Trans.* **2016**, *45*, 3236–3243.
[32] S. Raub, G. Jansen, *Theor. Chem. Acc.* **2001**, *106*, 223–232.
[33] A. Leithe-Jasper, Borrmann, H., Hönle, W., *In Scientific Report of the Max-Planck-Institute for Chemical Physics of Solids (MPI CPfS, Dresden, 2006)* **2003–2005**, 24–27.
[34] L. Akselrud, Y. Grin, *J. Appl. Crystallogr.* **2014**, *47*, 803–805.
[35] K. Koepernik, H. Eschrig, *Phys. Rev. B* **1999**, *59*, 1743.
[36] J. P. Perdew, Y. Wang, *Phys. Rev. B* **1992**, *45*, 13244.
[37] M. Kohout, *Int. J. Quantum Chem.* **2004**, *97*, 651–658.
[38] A. Ormeci, H. Rosner, F. Wagner, M. Kohout, Y. Grin, *J. Phys. Chem. A* **2006**, *110*, 1100–1105.
[39] M. Kohout, *DGrid, versions 4.6-5.0, Dresden* **2018–2021**.

Manuscript received: May 19, 2022
Revised manuscript received: June 1, 2022